Numerical continuation of boundaries in parameter space between stable and unstable periodic travelling wave (wavetrain) solutions of partial differential equations

Jonathan A. Sherratt

Abstract A variety of numerical methods are available for determining the stability of a given solution of a partial differential equation. However for a family of solutions, calculation of boundaries in parameter space between stable and unstable solutions remains a major challenge. This paper describes an algorithm for the calculation of such stability boundaries, for the case of periodic travelling wave solutions of spatially extended local dynamical systems. The algorithm is based on numerical continuation of the spectrum. It is implemented in a fully automated way by the software package WAVETRAIN, and two examples of its use are presented. One example is the Klausmeier model for banded vegetation in semi-arid environments, for which the change in stability is of Eckhaus (sideband) type; the other is the two-component Oregonator model for the photosensitive Belousov–Zhabotinskii reaction, for which the change in stability is of Hopf type.

J. A. Sherratt (✉)
Department of Mathematics and Maxwell Institute for Mathematical Sciences,
Heriot-Watt University, Edinburgh EH14 4AS, UK
e-mail: jas@ma.hw.ac.uk

1 Introduction

The stability of spatiotemporal solutions of partial differential equations (PDEs) is fundamental to their mathematical role and to their relevance in applications. There are various different notions of stability and throughout this paper I consider spectral stability, defined formally in Section 2 below. In some special cases (e.g. [1, 2]) this can be determined analytically. Otherwise one must rely on numerical calculation, and a number of numerical methods are available. For wave fronts and pulses, the most established method uses shooting to solve the eigenfunction equation (e.g. [3–7], http://www.amsta.leeds.ac.uk/˜jitse/software.html); the mismatch of solutions obtained by shooting from plus and minus infinity is characterised by the Evans function [8–10]. An alternative method due to Deconinck and coworkers [11, 12] is based on truncating the Fourier–Floquet expansion of the eigenfunction equation ("Hill's Method"). The method is particularly well suited to spatially periodic solutions, though it can be applied more generally, and a "black box" software package implementing the method is available at http://www.amath.washington.edu/hill/spectruw.html. A third method is due to Rademacher et al. [13], and involves numerical continuation of the spectrum using the (imaginary) spatial eigenvalue as a continuation parameter. This has been used successfully for both pulse wave and periodic travelling wave (PTW) solutions of reaction-diffusion systems [14–17], and for PTW solutions of other equation types [13, 18]. A quite different approach to the calculation of spectral stability involves pseudospectra [19]. Here one finds points in the eigenvalue complex plane for which the resolvent exceeds a threshold value; this provides an approximation to the spectrum.

These methods all concern the determination of (spectral) stability for a given PDE solution. However in applications it would often be desirable to calculate also curves in parameter space across which PDE solutions from a given family change stability. Plane wave solutions of the complex Ginzburg-Landau equation provide a rare example for which such curves can be calculated analytically, and the results have proved invaluable in understanding the complex spatiotemporal dynamics observed in numerical simulations of this equation (e.g. [20–22]). Numerically, one can of course obtain an approximation to such stability boundaries by calculating the stability of the solution family at a grid of points in parameter space. However numerical methods for more accurate calculation of stability boundaries are very limited. Rademacher et al. [13] discuss briefly the extension of their numerical continuation approach to detect certain types of stability change, and continue them in parameter space. In this paper I develop this idea further, presenting an algorithm for the numerical calculation of any stability boundary for PTW solutions of spatially extended local dynamical systems in one space dimension. Further, I demonstrate the implementation of the algorithm in the new software package WAVETRAIN [18].

2 Stability of periodic travelling waves

I consider PDEs of the form

$$J_i \, \partial u_i / \partial t = F_i \left(\underline{u}, \, \partial \underline{u} / \partial x, \, \partial^2 \underline{u} / \partial x^2, \dots \right) \tag{1}$$

$(1 \le i \le n)$. Here $\underline{u} \in \mathbb{R}^n$, and $J_i = 0$ or 1, with $J_i = 1$ for at least value of i.

Travelling wave solutions of (1) have the form $\underline{u}(x, t) = \underline{U}(z)$ where $z = x - ct$ with c being the wave speed. Such solutions satisfy

$$c \, \underline{M} \, d\underline{U} / dz + \underline{F} \left(\underline{U}, \, d\underline{U} / dz, \, d^2 \underline{U} / dz^2, \dots \right) = 0 \tag{2}$$

where $\underline{M}$ is an $n \times n$ matrix with diagonal $\underline{J}$ and with all off-diagonal entries zero. PTWs are limit cycle solutions of (2).

To study stability of PTWs, it is convenient to reformulate (1) in terms of z and t. Writing $\underline{u}(x, t) = \underline{\tilde{u}}(z, t)$, this gives

$$\underline{M} \, \partial \underline{\tilde{u}} / \partial t = c \, \underline{M} \, \partial \underline{\tilde{u}} / \partial z + \underline{F} \left(\underline{\tilde{u}}, \, \partial \underline{\tilde{u}} / \partial z, \, \partial^2 \underline{\tilde{u}} / \partial z^2, \dots \right) . \tag{3}$$

A PTW solution $\underline{U}_{ptw}(z)$ is an equilibrium solution of (3), and its spectrum is determined by the eigenfunction equation

$$\lambda \, \underline{M} \, \widehat{\underline{U}} = c \, \underline{M} \, \partial \widehat{\underline{U}} / \partial z + \nabla \underline{F} \, \widehat{\underline{U}} \tag{4}$$

where $\nabla \underline{F}$ denotes the Jacobian matrix of $\underline{F}$ with respect to $\underline{\tilde{u}}$ and its derivatives, evaluated at $\underline{U}_{ptw}$. Note that the eigenvalue λ and the eigenfunction $\widehat{\underline{U}}$ are complex-valued. Appropriate boundary conditions on $\widehat{\underline{U}}$ can be derived using Floquet theory [11, 13, 23] which implies that

$$\widehat{\underline{U}}(L) = \widehat{\underline{U}}(0) \exp(i\gamma) \quad \text{for some } \gamma \in \mathbb{R} \tag{5}$$

where L is the period of the PTW. Intuitively, the requirement that the eigenfunction is bounded for all $z \in \mathbb{R}$ means that its amplitude cannot change across one period of the PTW. However there is no restriction on the phase of the eigenfunction, except that each component must have the same change in phase across one period of the wave, since they are coupled in the linear eigenfunction equations. The spectrum $\mathcal{S} = \{ \lambda \mid (4) \text{ and } (5) \text{ have a non-trivial solution} \}$. In general the spectra of linear operators consist of a discrete part (the "point spectrum") and a continuous part (the "essential spectrum"). However for PTWs the point spectrum is always empty [23, Section 3.4.2], and the spectrum consists entirely of the (continuous) essential spectrum. The PTW solution $\underline{U}_{ptw}(z)$ is defined as spectrally stable if and only if all elements of $\mathcal{S}$ have $\operatorname{Re} \lambda \le 0$. Note that $0 \in \mathcal{S}$ in all cases; this reflects the neutral stability of the wave to translation.

There are two ways in which the stability of a PTW can change as either the PDE parameters or the wave speed c are varied [24]. An Eckhaus (sideband) stability change occurs when the curvature of the spectrum $\mathcal{S}$ at the origin changes sign, as illustrated in Fig. 1a. Alternatively, a fold in the spectrum can cross the imaginary axis at a point away from the origin (Fig. 1b); this is known as a stability change of Hopf type.
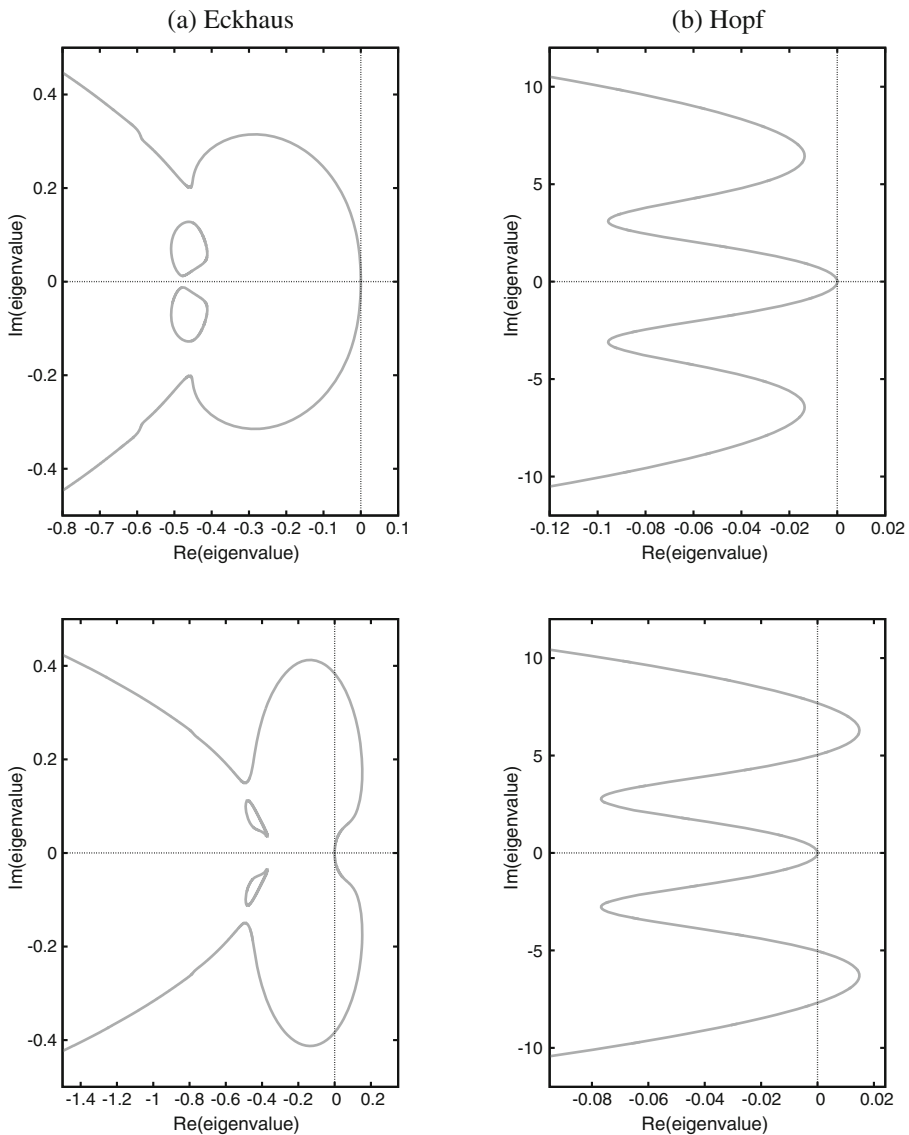
(a) Eckhaus

(b) Hopf

Fig. 1 Examples of spectra of PTWs on either side of a stability change of **a** Eckhaus type and **b** Hopf type. In **a** the spectra are for PTW solutions of (19) with $A = 1.0$, $B = 0.45$, $\nu = 182.5$ and $c = 0.7$ (*upper panel*), $c = 0.4$ (*lower panel*). In **b** the spectra are for PTW solutions of (20) with $\epsilon = 0.05$, $f = 2.1$, $\xi = 10^{-4}$, $q = 0.002$, $c = 9.85$ and $\phi = 8.21$ (*upper panel*), $\phi = 8.22$ (*lower panel*). The spectra were calculated and plotted using the software package WAVETRAIN (http://www.ma.hw.ac.uk/wavetrain). Full details of the WAVETRAIN input files, run commands and plot commands are given at http://www.ma.hw.ac.uk/˜jas/supplements/stabilityboundaries. Readers comparing my results on (20) with those in [14] should note that there is a small error in the legend of Fig. 12 in that paper. The value for $\xi\phi$ in Fig. 12b of [14] should be 8.22×10^{-4}, not 8.23×10^{-4} as stated. I am grateful to Grigory Bordyugov for confirming this in personal correspondence. The total run time for all of the various computations used for these plots was 56 min using a 2.83 GHz Intel Core 2 Quad Q9500 processor (see http://www. ma.hw.ac.uk/˜jas/supplements/stabilityboundaries for details)

3 The computational algorithm

The eigenfunction equation (4) can be rewritten as a system of first order ODEs:

$$dv/dz = \left[\underline{\underline{Y}}(z) + \lambda \, \underline{\underline{Z}} \right] \underline{v}. \tag{6}$$

Here $\underline{v}(z) \in \mathbb{R}^N$ where $N \geq n$ depends on the order of the derivatives in (4). $\underline{\underline{Y}}$ and $\underline{\underline{Z}}$ are $N \times N$ matrices, with $\underline{\underline{Y}}$ being a periodic function of z with period L, the period of the PTW. Following Rademacher et al. [13], I write $\underline{w}(z) = e^{-i\gamma z/L} \underline{v}(z)$ and $\zeta = z/L$, so that (6) becomes[1]

$$d\underline{w}/d\zeta = L \left[\underline{\underline{Y}}(\zeta) + \lambda \, \underline{\underline{Z}} \right] \underline{w} - i\gamma \underline{w} \tag{7}$$

subject to $\underline{w}(1) = \underline{w}(0)$. In order to uniquely specify $\underline{w}$, it is necessary to normalise the amplitude:

$$\langle \underline{w}, \underline{w} \rangle = 1 \tag{8}$$

and to apply a suitable phase-fixing condition (discussed in Section 4 below). The inner product is defined as

$$\langle \underline{h_1}, \underline{h_2} \rangle = \int_{\zeta=0}^{\zeta=1} \underline{h_1} \cdot \underline{h_2}^* \, d\zeta$$

with the asterisk denoting complex conjugation.

In the following, it will be necessary to consider $\underline{w}_\gamma$ and $\underline{w}_{\gamma\gamma}$, where the subscript $_\gamma$ denotes partial differentiation with respect to γ. These quantities satisfy

$$d\underline{w}_\gamma/d\zeta = L \left[\underline{\underline{Y}}(\zeta) + \lambda \, \underline{\underline{Z}} - i\gamma \underline{\underline{I}} \right] \underline{w}_\gamma + \left[L\lambda_\gamma \underline{\underline{Z}} - i \underline{\underline{I}} \right] \underline{w} \tag{9}$$

$$d\underline{w}_{\gamma\gamma}/d\zeta = L \left[\underline{\underline{Y}}(\zeta) + \lambda \, \underline{\underline{Z}} - i\gamma \underline{\underline{I}} \right] \underline{w}_{\gamma\gamma} + 2 \left[L\lambda_\gamma \underline{\underline{Z}} - i \underline{\underline{I}} \right] \underline{w}_\gamma$$
$$+ \, L\lambda_{\gamma\gamma} \underline{\underline{Z}} \, \underline{w} \tag{10}$$

subject to

$$\underline{w}_\gamma(1) = \underline{w}_\gamma(0) \tag{11}$$

$$\underline{w}_{\gamma\gamma}(1) = \underline{w}_{\gamma\gamma}(0). \tag{12}$$

Here $\underline{\underline{I}}$ is the $N \times N$ identity matrix. As formulated above, $\underline{w}_\gamma$ and $\underline{w}_{\gamma\gamma}$ are not uniquely determined because they can contain arbitrary components lying in

---

[1]Equation (3.11) in [13] corresponds to (7) in this paper, but contains a small error: a factor of L is included in the final term. Equations (3.12) in [13] are correspondingly incorrect. These errors actually have no effect on the calculation of Eckhaus points, which is the context in which these equations are considered in [13]; however they are important for the calculation of stability changes of Hopf type.

the null space of (7). To prevent this, I follow [13] and impose the orthogonality conditions

$$\langle \underline{w}, \underline{w}_\gamma \rangle = 0 \tag{13}$$

$$\langle \underline{w}, \underline{w}_{\gamma\gamma} \rangle = 0. \tag{14}$$

At changes of stability of Eckhaus type $\lambda = \mathrm{Re}\,\lambda_\gamma = \mathrm{Re}\,\lambda_{\gamma\gamma} = 0$, while at those of Hopf type $\mathrm{Re}\,\lambda = \mathrm{Re}\,\lambda_\gamma = 0$ with $\mathrm{Im}\,\lambda \neq 0$. Note that these conditions are necessary, but for sufficiency one must also add a transversality condition, namely that the derivative of $\mathrm{Re}\,\lambda$ with respect to the parameter being varied is non-zero.

The starting point for my algorithm is two parameters sets $\mathcal{P}_1$ and $\mathcal{P}_2$ such that a PTW solution exists for each, stable in one case and unstable in the other. Further, I require that these PTWs are on the same solution branch of (2). Note that $\mathcal{P}_1$ and $\mathcal{P}_2$ include both the PDE parameters and the wave speed c. For some equations there may be more than one PTW solution for a given set of PDE parameters and wave speed, due to folds in the solution branch. If this is the case then the parameter specifications $\mathcal{P}_1$ and $\mathcal{P}_2$ must also include the choice of PTW. Additionally, in the case of a stability change of Hopf type, my algorithm requires that $\mathcal{P}_1$ be sufficiently close to the stability boundary; this will be discussed below. Finally I comment that there is no requirement to know *a priori* whether the stability change is of Eckhaus or Hopf type.

Stage 1 The initial step is to calculate the PTW solution for parameter set $\mathcal{P}_1$. Usually the PTW will lie on a solution branch emanating from a Hopf bifurcation point, in which case it is most easily calculated via numerical continuation along the branch, starting from the Hopf bifurcation point [18, 25]. Note however that the solution branch containing the PTW may not have a Hopf bifurcation as an end point, for example if it connects two homoclinic solutions; an example of this is given in [26]. In such a case it will be necessary to provide a starting point for the continuation externally, for example via a PDE simulation.

Stage 2 Having calculated the PTW solution, one must then calculate the rescaled eigenfunction $\underline{w}$ for the zero eigenvalue. This eigenvalue corresponds to the neutral stability of the PTW to translations, and therefore the eigenfunction is proportional to the derivative of the PTW with respect to the travelling wave coordinate. Numerical differentiaton of the (numerically calculated) PTW solution does not usually give a sufficiently accurate approximation to the eigenfunction, but the numerical continuation in Stage 1 can be augmented to include equations for both the PTW and its derivative. Alternatively one can calculate solutions of (4) and (5) with $\gamma = 0$, including an approximation to the zero eigenvalue and the corresponding eigenvector, by discretising in z and using finite difference approximations for the derivatives [27–30].

Stage 3 This stage of the algorithm is described in [13]. When $\lambda = 0$, $\gamma = 0$ also and therefore one can take the eigenfunction $\underline{w}$ to be real; as mentioned above, it is in fact proportional to the derivative of the PTW. Therefore in (9), (10), (11) and (12) the equations for the unknown quantities $\text{Im}\,\lambda_\gamma$, $\text{Im}\,\underline{w}_\gamma$, $\text{Re}\,\lambda_{\gamma\gamma}$ and $\text{Re}\,\underline{w}_{\gamma\gamma}$ decouple. Here the vectors $\text{Im}\,\underline{w}_\gamma$ and $\text{Re}\,\underline{w}_{\gamma\gamma}$ each constitute Nm scalar unknowns, where m is the number of mesh points in the numerical discretisation used in the calculation of $\underline{w}$ in Stage 2. One now solves these decoupled equations, which can be done using Newton's method: as noted in [13], almost any initial guess will converge to the correct solution since the equations are linear in the unknowns.

Stage 4 Stages 1–3 provide the starting point for a numerical continuation in parameter space, searching for a change in stability of Eckhaus type. The equations to be continued are the travelling wave equation (2), the rescaled eigenfunction equation (7) (with $\lambda = \gamma = 0$), the imaginary part of (9), and the real part of (10). Continuation occurs along the PTW solution branch linking $\mathcal{P}_1$ and $\mathcal{P}_2$, and the principal continuation parameter must be one of the PDE parameters or the wave speed, as appropriate. Secondary continuation parameters must include $\text{Re}\,\lambda_{\gamma\gamma}$, and one searches for a zero of this variable along the PTW solution branch.

Stage 5A A zero of $\text{Re}\,\lambda_{\gamma\gamma}$ corresponds to a change in stability of Eckhaus type. If such a point is detected during Stage 4, one can fix $\text{Re}\,\lambda_{\gamma\gamma} = 0$, replace it as a continuation parameter by a second PDE parameter/the wave speed, and then perform a continuation that will trace out a two-parameter locus of Eckhaus points. Since $\mathcal{P}_1$ will typically be in the interior of the parameter region under consideration, this continuation will have to be performed twice, with opposite initial directions. This will generate the stability boundary as required, and the algorithm then terminates.

Stage 5B If $\text{Re}\,\lambda_{\gamma\gamma}$ remains of constant sign between $\mathcal{P}_1$ and $\mathcal{P}_2$, then the stability change must be of Hopf rather than Eckhaus type.

Stage 6 I mentioned previously the requirement that $\mathcal{P}_1$ be sufficiently close in parameter space to the stability change. This ensures that the spectrum at $\mathcal{P}_1$ contains at least one fold with strictly positive imaginary part, and that amongst such folds, that with the largest real part will cross the imaginary axis at the stability change, as one varies parameters between $\mathcal{P}_1$ and $\mathcal{P}_2$. One now locates this fold via numerical continuation of (2), (7) and (9); note that both the real and imaginary parts of (9) must be considered, in contrast to the situation in Stage 3. The principal continuation parameter is γ, and secondary continuation parameters must include $\text{Re}\,\lambda_\gamma$: this is zero at a fold. Of course there may be many such folds, and it is the fold with the largest real part and strictly positive imaginary part that is of interest. In practice one restricts attention to the part of the spectrum with $\text{Re}\,\lambda$ greater than a suitable (negative) lower limit.

There are two basic problems with this continuation process: it is potentially very time-consuming, and one requires an appropriate starting point. Both of these problems can be overcome by first performing a numerical continuation of (2) and (7) alone, again with γ as the principal continuation parameter, tracing out the spectrum. From this one can determine the approximate location of the required fold, enabling the subsequent continuation of (2), (7) and (9) to be confined to a small region of the spectrum. Moreover the initial numerical continuation of (2) and (7) alone generates estimates of the derivatives of λ, $\underline{w}$ and γ along the solution branch, from which initial solutions for λ_γ and $\underline{w}_\gamma$ can be obtained.

Stage 7 The calculations in Stage 6 determine a point in the spectrum of the PTW at $\mathcal{P}_1$ with $\mathrm{Re}\,\lambda_\gamma = 0$, which will cross the imaginary axis along the PTW solution branch between $\mathcal{P}_1$ and $\mathcal{P}_2$. This crossing point corresponds to a stability change of Hopf type, and one locates it by numerical continuation of (2), (7) and (9), with the principal continuation parameter being one of the PDE parameters or the wave speed, as appropriate. Secondary continuation parameters must include $\mathrm{Re}\,\lambda$, and one searches for a point on the solution branch at which $\mathrm{Re}\,\lambda = 0$.

Stage 8 In Stage 7, one has determined a parameter set at which there is a stability change of Hopf type. This can be used as a starting point for calculating a two parameter locus of such points, by fixing $\mathrm{Re}\,\lambda = 0$ and replacing $\mathrm{Re}\,\lambda$ as a secondary continuation parameter by a second PDE parameter/the wave speed. As in Stage 5A, this continuation must be performed twice, with opposite initial directions, since $\mathcal{P}_1$ is (usually) in the interior of the parameter region under consideration.

The early stages of this algorithm have been used previously to calculate stability boundaries of Eckhaus type [16, 31]. However Stages 5B-8 are new, and their integration into a single unified algorithm provides a comprehensive approach to the calculation of stability boundaries. Note that the difference in stability between the PTWs at $\mathcal{P}_1$ and $\mathcal{P}_2$ does not guarantee that the change in stability between them is unique; there could be any odd number of stability changes. The algorithm described above will determine the locus of the stability change closest to $\mathcal{P}_1$.

4 Computational implementation

WAVETRAIN is a new software package, written by JAS, that provides a suite of commands for studying PTW solutions of PDEs. It is freely available and open-source (though protected by copyright), and can be downloaded from http://www.ma.hw.ac.uk/wavetrain. All of the WAVETRAIN commands are based on numerical continuation, which is performed using AUTO (http://indy.cs.concordia.ca/auto, [32–34]). The interface with AUTO is via

UNIX shell scripts, which does not cause any reduction in computational performance. A general description of WAVETRAIN has been given previously [18]. However that paper deliberately omitted any technical details of the command `stability_boundary`, which implements the algorithm given in Section 3 in a fully automated way. In the WAVETRAIN input files, the user specifies one of the PDE parameters as "control parameter", and fixes the values of the others. The arguments to the `stability_boundary` command then specify two pairs of control parameter and wave speed values lying either side of the stability boundary, and the command calculates the stability boundary in the control parameter–wave speed plane. In this section I summarise key points of computational detail in the implementation by WAVETRAIN of the algorithm in Section 3.

Stage 1 This is a straightforward numerical continuation; the user can specify either a parameter range in which WAVETRAIN searches for a Hopf bifurcation in the travelling wave equations (2), or a starting PTW solution.

Stage 2 WAVETRAIN discretises (4) and (5) in z with $\gamma = 0$, and solves the resulting matrix eigenvalue problem using routines from LAPACK (http://www.netlib.org/lapack, [35]). The order of the finite difference scheme used for the derivatives is specified by the user. The numerical mesh is inherited from the continuation of the PTW solution and is therefore non-uniform, and finite difference weights are calculated using Fornberg's algorithm [36]. In some cases (e.g. Example 2 in Section 5 below) run times can be significantly reduced by increasing the order of the finite difference scheme. Note that since it is only the eigenvector corresponding to $\lambda = 0$ that is required in this stage, the calculation of a large number of other eigenvalues and eigenfunctions that also have $\gamma = 0$ is highly inefficient; however the results are used in Stage 6 below, in the case of a stability change of Hopf type.

Stage 3 Following [13], WAVETRAIN implements the Newton's method solution of (4), Re (7), Im (9), Re (10), Im (11) and Re (12) by performing a continuation of these equations and boundary conditions in a dummy parameter. As mentioned in Section 3, the normalisation condition (8) must be supplemented by a phase-fixing condition for $\underline{w}$. This is because the boundary conditions for $\underline{w}$ are periodic and therefore permit an arbitrary phase shift. WAVETRAIN again follows [13], using

$$\text{Im} \left\langle \underline{w}_{\text{old}}, \underline{w} \right\rangle = 0 \,. \tag{15}$$

Here the subscript $_{\text{old}}$ denotes the solution at a previous continuation step. Intuitively, (15) implies that the phase of $\underline{w}$ does not change between successive continuation steps. In order that the PTW solution is determined uniquely, an integral condition is also imposed on $\underline{U}_{ptw}$:

$$\int_{z=0}^{z=L} \left(d\underline{U}_{ptw,\,\text{old}}/dz \right) \cdot \left(\underline{U}_{ptw,\,\text{old}} - \underline{U}_{ptw} \right) = 0 \,. \tag{16}$$

A phase-fixing condition such as this is required to prevent the PTW solution containing an arbitrary translation with respect to z. Condition (16) is used in the HOMCONT extension of AUTO [37]; more recent applications are given in [13, 16, 38, 39]. Intuitively, (16) states that the change in $\underline{U}_{ptw}$ between continuation steps is orthogonal to the change due to a small translation in z.

Since there are $5N$ real equations with $5N$ (periodic) boundary conditions and the 5 integral constraints (13), (14), (8), (15) and (16), AUTO requires 6 continuation parameters. For these, WAVETRAIN uses $\text{Re}\,\lambda$, $\text{Im}\,\lambda$, $\text{Im}\,\lambda_\gamma$, $\text{Re}\,\lambda_{\gamma\gamma}$ and L, in addition to the dummy parameter. Here and in all of the subsequent numerical continuations, the AUTO parameter ITNW is set to 7 rather than 5, which is recommended for "hard" problems. Also L, $\text{Re}\,\lambda_{\gamma\gamma}$, $\text{Im}\,\underline{w}_\gamma$ and $\text{Re}\,\underline{w}_{\gamma\gamma}$ are excluded from the pseudo-arclength calculation; this is helpful because these quantities can be very large, an issue also noted in [13]. A possible alternative strategy might be to use logarithms of these quantities to avoid large values; an example of this approach is given in [40]. In some cases the eigenfunction $\widehat{U} \in \mathbb{R}^n$ is a subset of $\underline{v} \in \mathbb{R}^N$; this depends on the way in which the first order ODEs (6) are formulated. In such a case, Rademacher et al. [13] recommend replacing (13) and (14) by the alternative conditions

$$\langle \widehat{\underline{w}}, \widehat{\underline{w}}_\gamma \rangle = 0 \tag{17}$$

$$\langle \widehat{\underline{w}}, \widehat{\underline{w}}_{\gamma\gamma} \rangle = 0 \tag{18}$$

where $\widehat{\underline{w}} \in \mathbb{R}^n$ is composed of the n components of $\underline{w}$ for which $\widehat{U}$ matches $\underline{v}$. These alternative conditions also ensure that $\underline{w}_\gamma$ and $\underline{w}_{\gamma\gamma}$ are orthogonal to the null space of (7). One of the WAVETRAIN input parameters specifies whether (13), (14) or (17), (18) are to be used; the examples in Section 5 both use the latter conditions.

Stages 4 and 5A   Having established the numerical continuation framework in Stage 3, Stages 4 and 5A are straightforward. One of either the control parameter or the wave speed replaces the dummy parameter as the principal continuation parameter in Stage 4, and the other replaces $\text{Re}\,\lambda_{\gamma\gamma}$ as a secondary continuation parameter in Stage 5A.

Stage 6   The first step in this stage is a numerical continuation of (2) and (7) using γ as the principal continuation parameter. A starting point for this is provided by the eigenvalues and eigenfunctions with $\gamma = 0$ that were calculated in Stage 2. WAVETRAIN performs a separate continuation starting from each of a user-specified number of these eigenvalues, ordered by their real part. The principal continuation parameter is γ with secondary continuation parameters being $\text{Re}\,\lambda$, $\text{Im}\,\lambda$ and L; this is the required number of continuation parameters since there are $3N$ equations, $3N$ (periodic) boundary conditions, and the integral constraints (8), (15) and (16). This preliminary continuation is used to determine a suitable small range for the more computationally intensive continuation of (2), (7) and (9), and also to provide suitable starting solutions

for λ_γ and $\underline{w}_\gamma$. AUTO performs continuations with respect to pseudo-arclength $\mathcal{A}$, and the output files from the preliminary continuation include (numerical approximations to) $\partial\lambda/\partial\mathcal{A}$, $\partial\underline{w}/\partial\mathcal{A}$ and $\partial\gamma/\partial\mathcal{A}$. A starting value for λ_γ can therefore be obtained immediately as $(\partial\lambda/\partial\mathcal{A})/(\partial\gamma/\partial\mathcal{A})$. However for $\underline{w}_\gamma$ one must take account of the fact that $\partial\underline{w}/\partial\mathcal{A}$ will in general not satisfy the orthogonality condition (13). Therefore a suitable starting solution is

$$\frac{\partial\underline{w}/\partial\mathcal{A}}{\partial\gamma/\partial\mathcal{A}} - K\underline{w} \quad \text{where } K = \left\langle \frac{\partial\underline{w}/\partial\mathcal{A}}{\partial\gamma/\partial\mathcal{A}}, \underline{w} \right\rangle \in \mathbb{R}.$$

Having obtained this starting solution, one can proceed with the continuation of (2), (7) and (9), a total of $5N$ real equations which are subject to $5N$ (periodic) boundary conditions and the 5 integral constraints (8), (15), (16), and either (13), (14) or (17), (18). The principal continuation parameter is γ, with secondary continuation parameters $\text{Re}\,\lambda$, $\text{Im}\,\lambda$, $\text{Re}\,\lambda_\gamma$, $\text{Im}\,\lambda_\gamma$ and L. WAVETRAIN excludes L, $\text{Im}\,\lambda_\gamma$ and $\underline{w}_\gamma$ from the pseudo-arclength calculation in this continuation and those in Stages 7 and 8, since these quantities can be large. An additional advantage of these exclusions, together with the corresponding exclusions in Stages 3-5A, is that the pseudo-arclengths associated with stability changes of Eckhaus and Hopf type are directly comparable, and thus the same step sizes can be used for the two cases.

Stages 7 and 8 Having established the numerical continuation framework in Stage 6, Stages 7 and 8 are straightforward. In Stage 7, either the control parameter or the wave speed replaces γ as the principal continuation parameter, and γ replaces $\text{Re}\,\lambda_\gamma$ as a secondary continuation parameter. In Stage 8, the other of the control parameter or wave speed replaces $\text{Re}\,\lambda$ as a secondary continuation parameter.

5 Examples

5.1 Example 1: the Klausmeier model

When suitably nondimensionalised, the Klausmeier model for vegetation dynamics in semi-arid environments is

$$\partial p/\partial t = \omega p^2 - Bp + \partial^2 p/\partial x^2 \tag{19a}$$

$$\partial w/\partial t = A - \omega - \omega p^2 + \nu\,\partial\omega/\partial x \tag{19b}$$

[41]. Here $p(x, t)$ and $\omega(x, t)$ represent plant and water densities at time t and position x in a one-dimensional domain that is a gentle slope of constant gradient; x increases in the uphill direction. A, B and ν are positive constants. Plant growth is proportional to water uptake, which has a nonlinear dependence on plant density. This reflects the positive correlation between infiltration of rain water into the soil and vegetation biomass, which results from higher levels of organic matter in the soil, and from the presence of roots [42–45]. Plant spread

via seed dispersal is represented by linear diffusion. The plant loss term Bp represents both natural death and herbivory. Water falls as rain at an average rate A, is lost by evaporation, and flows downhill; the parameter ν reflects the steepness of the slope.

The Klausmeier model is used to study banded vegetation patterns, which are a characteristic feature of gentle slopes in semi-deserts. These patterns comprise alternating stripes of vegetation and bare ground running parallel to the contours. They are self-organised, and most data indicates that they move slowly uphill [45, 46, Chapter 10]. This migration is thought to arise from moisture levels being higher on the uphill edge of the bands than the downhill edge, resulting in reduced plant death and greater seedling density [47, 48]. Ecological details of banded vegetation are reviewed in [45]. Mathematical details of the Klausmeier model are discussed in [49–52]. Ptw stability in an amended version of (19), with a diffusion term added to (19b), is considered in [53], and ptw stability has also been considered for the Gray-Scott model, which has similar kinetics to (19) [54]. Alternative mathematical models based on different ecological assumptions are given in [55–59].

The solutions of the Klausmeier model corresponding to banded vegetation are spatial patterns moving at a constant speed in the positive x direction, i.e. ptws. With B and ν fixed at ecologically typical values [41], (19) has a ptw solution for a wide range of values of the rainfall parameter A and the wave speed c [60]. Figure 2 illustrates the division of part of the A–c parameter plane into stable ptws, unstable ptws, and no ptws. The stability boundary is of Eckhaus type (see Fig. 1a), and was calculated using the algorithm I have described, as implemented by WAVETRAIN's `stability_boundary` command. The required initial pairs of control parameter and wave speed values were obtained by experimental testing of stability across the parameter plane. Any of the methods discussed in Section 1 can be used for this; I used the WAVETRAIN command `stability` which implements the method of Rademacher et al. [13].

5.2 Example 2: the two-component Oregonator model

The Belousov–Zhabotinskii reaction exhibits a wide variety of spatiotemporal dynamics [61–63] including one-dimensional ptws [64]. The two component Oregonator model

$$\partial\alpha/\partial t = \partial^2\alpha/\partial x^2 + (1/\epsilon)\left[\alpha - \alpha^2 - (f\beta + \xi\phi)(\alpha - q)/(\alpha + q)\right] \quad (20a)$$

$$\partial\beta/\partial t = \alpha - \beta \tag{20b}$$

is a simplified dimensionless representation of the photosensitive variant of the reaction [14, 65]. Here $\alpha(x, t)$ and $\beta(x, t)$ represent the concentrations of bromous acid and the oxidised form of the catalyst respectively, at time t and spatial location x in a one-dimensional domain; ϵ, f, ξ, ϕ and q are positive constants. Equations (20) follow from a quasi-steady state reduction of a three
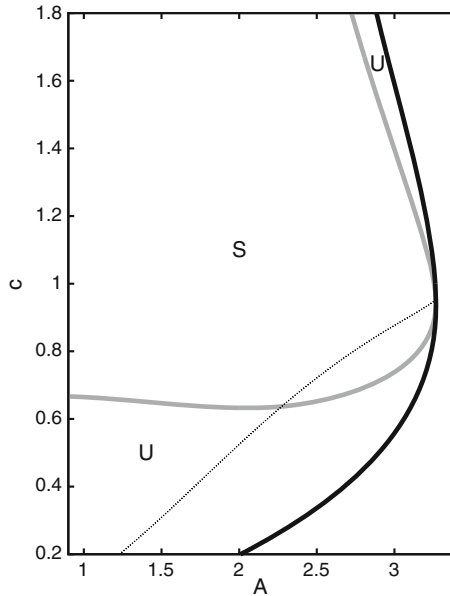
Fig. 2 The boundary between stable (*S*) and unstable (*U*) PTW solutions of (19) (*thick grey curve*). The stability change between these regions is of Eckhaus type (see Fig. 1a). Also plotted is a locus of Hopf bifurcation points in the travelling wave equations (*thick black curve*), and a curve along which there is a PTW solution with constant period 14.74 (*thin black dotted curve*). The Hopf bifurcation of the travelling wave equations is supercritical in this part of the *A*–*c* plane, and to the right of the Hopf bifurcation locus there are no PTW solutions. There is exactly one PTW solution throughout the part of the parameter plane shown, to the left of the Hopf bifurcation locus. The parameter values are $B = 0.45$ and $\nu = 182.5$. The curves were calculated and plotted using the software package WAVETRAIN (http://www.ma.hw.ac.uk/wavetrain). Full details of the WAVETRAIN input files, run commands and plot commands are given at http://www.ma.hw.ac.uk/˜jas/supplements/stabilityboundaries. The total run time for all of the various computations used for this plot was 30 min using a 2.83 GHz Intel Core 2 Quad Q9500 processor (see http://www.ma.hw.ac.uk/˜jas/supplements/stabilityboundaries for details)

variable model, with $(f\beta + \xi\phi)/(\alpha + q)$ being the quasi-steady concentration of bromide; $\xi\phi$ is the rate of bromide release due to light absorption. The constant $\xi = 10^{-4}$ is included so that ϕ has a similar size to the wave speed c; this is helpful when performing two-parameter continuation in ϕ and c. The constant f is a stoichiometric factor reflecting the production rate of bromide per unit of reduced catalyst.

Mathematical properties of PTW solutions of (20) are discussed by Bordiougov and Engel [14]. Their paper includes computations of the spectrum of PTW solutions of (20) which suggest that as the parameter ϕ is varied, the waves can undergo a change in stability of Hopf type. Their results provide starting parameter sets $\mathcal{P}_1$ and $\mathcal{P}_2$ for my algorithm, and using WAVETRAIN's `stability_boundary` command I traced the stability boundary in the ϕ–c plane (Fig. 3).
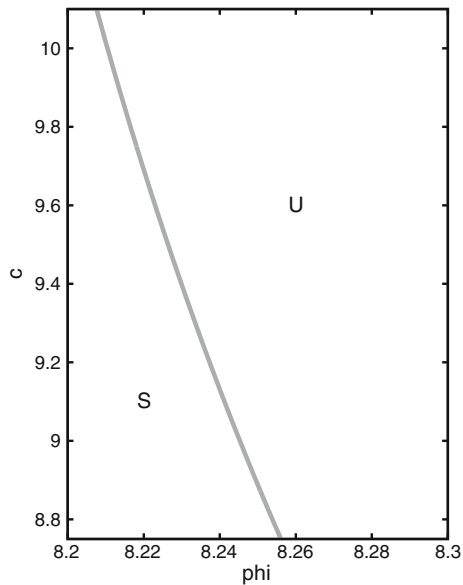
Fig. 3 The boundary between stable (S) and unstable (U) PTW solutions of (20). The stability change between these regions is of Hopf type (see Fig. 1b). The parameter values are $\epsilon = 0.05$, $f = 2.1$, $\xi = 10^{-4}$, $q = 0.002$. There is exactly one PTW solution throughout the part of the parameter plane shown. The stability boundary was calculated and plotted using the software package WAVETRAIN (http://www.ma.hw.ac.uk/wavetrain). Full details of the WAVETRAIN input files, run commands and plot commands are given at http://www.ma.hw.ac.uk/~jas/supplements/stabilityboundaries. The total run time for all of the various computations used for this plot was 3.5 h using a 2.83 GHz Intel Core 2 Quad Q9500 processor (see http://www.ma.hw.ac.uk/~jas/supplements/stabilityboundaries for details)

6 Application of stability boundaries: an example

I conclude by giving a brief example of a way in which the calculation of a stability boundary for PTWS can be helpful in understanding PDE dynamics. I return to the Klausmeier model (19). Sherratt and Lord [60] have demonstrated hysteresis in the wavelength (spatial period) of observed patterns as the rainfall parameter A is varied. This is illustrated in Fig. 4, in which I plot results from a numerical simulation of (19) on a domain of length 100 with periodic boundary conditions. I decreased A slowly from an initial value that is just below the upper threshold for patterning, which is 3.265 on this domain. A PTW of wavelength 14.286 (mode 7) develops initially. As A is decreased further, the form of the pattern (PTW) changes but its wavelength remains constant, until it switches to 20 (mode 5) at $A = 1.9$. When A is then increased again, the pattern wavelength remains at 20.

In the field, banded vegetation patterns typically occur over regions spanning many wavelengths. Therefore one is primarily interested in the effects of rainfall variation for spatial domains that can be reasonably approximated as infinite. If the rainfall parameter A is gradually decreased on an infinite
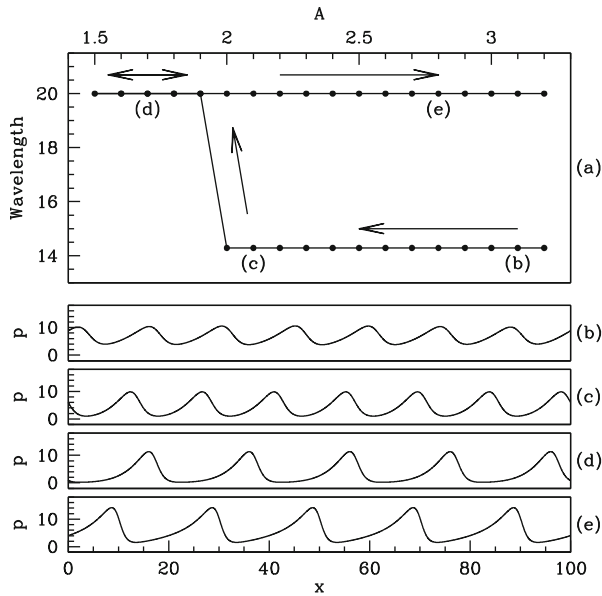
Fig. 4 A numerical simulation of the Klausmeier model (19) with slow variation in the rainfall parameter A, demonstrating hysteresis. The other parameter values were $B = 0.45$ and $\nu = 182.5$. The boundary conditions were periodic in p and ω. The parameter A was changed in steps of 0.1, with 200 time units between changes, and the average spatial wavelength of the pattern was measured immediately prior to the decrease. Initially, A was set to 3.2, with $p(x, 0) = p_s [1 + 0.1\delta_p(x)]$, $\omega(x, 0) = \omega_s [1 + 0.1\delta_\omega(x)]$. Here (p_s, ω_s) is the unique locally stable steady state with $p_s \neq 0$ (see [50] for details). The quantities δ_p, $\delta_\omega \in [0, 1]$ denote spatial noise, chosen randomly and independently from a uniform distribution at each numerical grid point. **a** shows the variation in the average spatial wavelength of the solution, measured immediately prior to the next change in A. **b–e** show the solutions for p at the four values of A indicated in **a**; again, these were recorded immediately prior to the next change in A. For **d**, the solution was recorded during the part of the solution in which A was increasing. The arrows indicate the direction of change in A. The equations were solved using a finite difference scheme applying upwinding to the convective term, with a uniform grid spacing of 2.5×10^{-2} and a time step of 1.096×10^{-4}; these give a Courant number of 0.8. These discretisations are chosen to give errors of less than 1% in both p and ω throughout the solution. The simulation took 13 h using a 2.83 GHz Intel Core 2 Quad Q9500 processor

domain, PTWs will first develop at $A = 3.267$, which corresponds to the fold in the Hopf bifurcation locus (see Fig. 2). The corresponding wavelength is 14.74, and the locus on which PTWs have this wavelength is plotted in Fig. 2. As A is decreased slowly, one expects the solution to remain on this locus until it becomes unstable. This occurs when the locus crosses the PTW stability boundary, at $A = 2.275$ (see Fig. 2). Note that this is significantly larger than the threshold seen in Fig. 4. The threshold is of course slightly affected by the small difference in the wavelength of the waves being considered. However the difference between the two threshold levels of A is due mainly to two other factors. Firstly the region of stable PTWs is larger on the finite domain, because the boundary conditions restrict the spatial eigenvalues that are admissible.

Secondly, the finiteness of the time interval between changes in A in the simulations means that very slowly growing modes are not detected.

The ability to predict accurately the rainfall level at which pattern wavelength will shift using numerical continuation is valuable since long time numerical studies on large domains are very expensive. For instance, I attempted to calculate the critical value $A = 2.275$ to an accuracy of just one decimal place via simulations of the type used in Fig. 4. This required sufficiently large domain lengths and time intervals that the run times for each individual simulation took about a week (with numerical method and processor as given in the legend to Fig. 4). In comparison, using WAVETRAIN one can calculate the threshold to four decimal places in about 15 min.

References

1. Kopell, N., Howard, L.N.: Plane wave solutions to reaction–diffusion equations. Stud. Appl. Math. **52**, 291–328 (1973)
2. Aranson, I.S., Kramer, L.: The world of the complex Ginzburg–Landau equation. Rev. Modern Phys. **74**, 99–143 (2002)
3. Bridges, T.J., Derks, G., Gottwald, G.: Stability and instability of solitary waves of the fifth-order KdV equation: a numerical framework. Physica D **172**, 190–216 (2002)
4. Coombes, S., Owen, M.R.: Evans functions for integral neural field equations with Heaviside firing rate function. SIAM J. Appl. Dyn. Syst. **34**, 574–600 (2004)
5. Aparicio, N.D., Malham, S.J.A., Oliver, M.: Numerical evaluation of the Evans function by Magnus integration. BIT **45**, 219–258 (2005)
6. Ledoux, V., Malham, S.J.A., Niesen, J., Thümmler, V.: Computing stability of multi-dimensional travelling waves. SIAM J. Appl. Dyn. Syst. **8**, 480–507 (2009)
7. Ledoux, V., Malham, S.J.A., Thümmler, V.: Grassmannian spectral shooting. Math. Comput. **79**, 1585–1619 (2010)
8. Evans, J.W.: Nerve axon equations: IV The stable and unstable pulse. Indiana Univ. Math. J. **24**, 1169–1190 (1975)
9. Alexander, J., Gardner, R., Jones, C.: A topological invariant arising in the stability analysis of travelling waves. J. Reine Angew. Math. **410**, 167–212 (1990)
10. Gardner, R.A.: On the structure of the spectra of periodic travelling waves. J. Math. Pures Appl. **72**, 415–439 (1993)
11. Deconinck, B., Kutz, J.N.: Computing spectra of linear operators using the Floquet–Fourier–Hill method. J. Comput. Phys. **219**, 296–321 (2006)
12. Deconinck, B., Kiyak, F., Carter, J.D., Kutz, J.N.: SpectrUW: a laboratory for the numerical exploration of spectra of linear operators. Math. Comput. Simul. **74**, 370–379 (2007)
13. Rademacher, J.D.M., Sandstede, B., Scheel, A.: Computing absolute and essential spectra using continuation. Physica D **229**, 166–183 (2007)
14. Bordiougov, G., Engel, H.: From trigger to phase waves and back again. Physica D **215**, 25–37 (2006)
15. Röder, G., Bordyugov, G., Engel, H., Falcke, M.: Wave trains in an excitable FitzHugh–Nagumo model: bistable dispersion relation and formation of isolas. Phys. Rev. E **75**(3), 036202 (2007)

16. Smith, M.J., Sherratt, J.A.: The effects of unequal diffusion coefficients on periodic travelling waves in oscillatory reaction–diffusion systems. Physica D **236**, 90–103 (2007)
17. Sherratt, J.A., Smith, M.J.: Periodic travelling waves in cyclic populations: field studies and reaction-diffusion models. J. R. Soc. Interface **5**, 483–505 (2008)
18. Sherratt, J.A.: Numerical continuation methods for studying periodic travelling wave (wavetrain) solutions of partial differential equations. Appl. Math. Comput. **218**, 4684–4694 (2012)
19. Trefethen, L.N., Embree, M.: Spectra and Pseudospectra: The Behavior of Nonnormal Matrices and Operators. Princeton University Press, Princeton (2005)
20. Janiaud, B., Pumir, A., Bensimon, D., Croquette, V., Richter, H., Kramer, L.: The Eckhaus instability for traveling waves. Physica D **55**, 269–286 (1992)
21. Brusch, L., Torcini, A., van Hecke, M., Zimmermann, M.G., Bär, M.: Modulated amplitude waves and defect formation in the one-dimensional complex Ginzburg–Landau equation. Physica D **160**, 127–148 (2001)
22. Sherratt, J.A., Smith, M.J., Rademacher, J.D.M.: Locating the transition from periodic oscillations to spatiotemporal chaos in the wake of invasion. Proc. Natl. Acad. Sci. USA **106**, 10890–10895 (2009)
23. Sandstede, B.: Stability of travelling waves. In: Fiedler, B. (ed.) Handbook of Dynamical Systems II, pp. 983–1055. North-Holland, Amsterdam (2002)
24. Rademacher, J.D.M., Scheel, A.: Instabilities of wave trains and Turing patterns in large domains. Int. J. Bifur. Chaos **17**, 2679–2691 (2007)
25. Doedel, E.J., Kernevez, J.P.: A numerical analysis of wave phenomena in a reaction diffusion model. In: Othmer, H.G. (ed.) Nonlinear Oscillations in Biology and Chemistry (Lecture Notes in Biomathematics 66), pp. 261–273. Springer, Berlin (1986)
26. Doedel, E.J., Kernevez, J.P.: Auto: software for continuation and bifurcation problems in ordinary differential equations. Applied Mathematics Report, California Institute of Technology, Pasadena (1986). See also pp. 374–388 of http://cmvl.cs.concordia.ca/courses/comp-6361/fall-2011/notes.pdf
27. Atkinson, F.V.: Discrete and Continuous Boundary Problems. Academic, New York (1964)
28. Kreiss, H.O.: Difference approximation for boundary and eigenvalue problems for ordinary differential equations. Math. Comput. **26**, 605–624 (1972)
29. de Boor, C., Swartz, B.: Collocation approximation to eigenvalues of an ordinary differential equation: the principle of the thing. Math. Comput. **35**, 679–694 (1980)
30. Chatelin, F.: The spectral approximation of linear operators with applications to the computation of eigenelements of differential and integral operators. SIAM Rev. **23**, 495–522 (1981)
31. Merchant, S.M.: Spatiotemporal patterns in mathematical models for predator invasions. PhD thesis, University of British Columbia (2009). http://www.iam.ubc.ca/theses/SandraMerchant/SMerchant_PhD_Thesis.pdf
32. Doedel, E.J.: Auto, a program for the automatic bifurcation analysis of autonomous systems. Cong. Numer. **30**, 265–384 (1981)
33. Doedel, E.J., Keller, H.B., Kernévez, J.P.: Numerical analysis and control of bifurcation problems: (I) bifurcation in finite dimensions. Int. J. Bifurc. Chaos **1**, 493–520 (1991)
34. Doedel, E.J., Govaerts, W., Kuznetsov, Y.A., Dhooge, A.: Numerical continuation of branch points of equilibria and periodic orbits. In: Doedel, E.J., Domokos, G., Kevrekidis, I.G. (eds.) Modelling and Computations in Dynamical Systems, pp. 145–164. World Scientific, Singapore (2006)
35. Anderson, E., Bai, Z., Bischof, C., Blackford, S., Demmel, J., Dongarra, J., Du, J., Croz, Greenbaum, A., Hammarling, S., McKenney, A., Sorensen, D.: Lapack Users' Guide, 3rd edn. Society for Industrial and Applied Mathematics, Philadelphia (1999)
36. Fornberg, B.: Calculation of weights in finite difference formulas. SIAM Rev. **40**, 685–691 (1998)
37. Champneys, A.R., Kuznetsov, Y.A., Sandstede, B.: A numerical toolbox for homoclinic bifurcation analysis. Int. J. Bifur. Chaos **6**, 867–887 (1996)
38. Dawes, J.H.P.: Localized pattern formation with a large-scale mode: slanted snaking. SIAM J. Appl. Dyn. Syst. **7**, 186–206 (2008)
39. Dawes, J.H.P.: Modulated and localized states in a finite domain. SIAM J. Appl. Dyn. Syst. **8**, 909–930 (2009)
40. Doedel, E.J., Kooi, B.W., Van Voorn, G.A.K., Kuznetsov, Y.A.: Continuation of connecting orbits in 3D-ODEs: (II) cycle-to-cycle connections. Int. J. Bifurc. Chaos **19**, 159–169 (2009)

41. Klausmeier, C.A.: Regular and irregular patterns in semiarid vegetation. Science **284**, 1826–1828 (1999)
42. Callaway, R.M.: Positive interactions among plants. Bot. Rev. **61**, 306–349 (1995)
43. Hills, R.C.: The influence of land management and soil characteristics on infiltration and the occurrence of overland flow. J. Hydrol. **13**, 163–181 (1971)
44. Rietkerk, M., Ketner, P., Burger, J., Hoorens, B., Olff, H.: Multiscale soil and vegetation patchiness along a gradient of herbivore impact in a semi-arid grazing system in West Africa. Plant Ecol. **148**, 207–224 (2000)
45. Valentin, C., d'Herbès, J.M., Poesen, J.: Soil and water components of banded vegetation patterns. Catena **37**, 1–24 (1999)
46. Deblauwe, V.: Modulation des structures de végétation auto-organisées en milieu aride [trans: self-organized vegetation pattern modulation in arid climates]. PhD thesis, Université Libre de Bruxelles. http://theses.ulb.ac.be/ETD-db/collection/available/ULBetd-04122010-093151/ (2010)
47. Montaña, C., Seghieri, J., Cornet, A.: Vegetation dynamics: recruitment and regeneration in two-phase mosaics. In: Tongway, D.J., Valentin, C., Seghieri, J. (eds.) Banded Vegetation Patterning in Arid and Semi-Arid Environments, pp. 132–145. Springer, New York (2001)
48. Tongway, D.J., Ludwig, J.A.: Theories on the origins, maintainance, dynamics, and functioning of banded landscapes. In: Tongway, D.J., Valentin, C., Seghieri, J. (eds.) Banded Vegetation Patterning in Arid and Semi-Arid Environments, pp. 20–31. Springer, New York (2001)
49. Sherratt, J.A.: Pattern solutions of the Klausmeier model for banded vegetation in semi-arid environments II: patterns with the largest possible propagation speeds. Proc. R. Soc. Lond. A **467**, 3272–3294 (2011)
50. Sherratt, J.A.: An analysis of vegetation stripe formation in semi-arid landscapes. J. Math. Biol. **51**, 183–197 (2005)
51. Sherratt, J.A.: Pattern solutions of the Klausmeier model for banded vegetation in semi-arid environments I. Nonlinearity **23**, 2657–2675 (2010)
52. Sherratt, J.A.: Pattern solutions of the Klausmeier model for banded vegetation in semi-arid environments III: the transition between homoclinic solutions (2012, submitted)
53. van der Stelt, S., Doelman, A., Hek, G., Rademacher, J.D.M.: Rise and fall of periodic patterns for a generalized Klausmeier–Gray–Scott model. J. Nonlinear Sci. (2012). doi:10.1007/s00332-012-9139-0
54. Doelman, A., Rademacher, J.D.M., van der Stelt, S.: Hopf dances near the tips of Busse balloons. Discrete Continuous Dyn. Syst., Ser. S **5**, 61–92 (2012)
55. Lefever, R., Lejeune, O.: On the origin of tiger bush. Bull. Math. Biol. **59**, 263–294 (1997)
56. HilleRisLambers, R., Rietkerk, M., van de Bosch, F., Prins, H.H.T., de Kroon, H.: Vegetation pattern formation in semi-arid grazing systems. Ecology **82**, 50–61 (2001)
57. von Hardenberg, J., Meron, E., Shachak, M., Zarmi, Y.: Diversity of vegetation patterns and desertification. Phys. Rev. Lett. **87**(19), 198101 (2001)
58. Rietkerk, M., Boerlijst, M.C., van Langevelde, F., HilleRisLambers, R., van de Koppel, J., Prins, H.H.T., de Roos, A.: Self-organisation of vegetation in arid ecosystems. Am. Nat. **160**, 524–530 (2002)
59. Gilad, E., von Hardenberg, J., Provenzale, A., Shachak, M., Meron, E.: A mathematical model of plants as ecosystem engineers. J. Theor. Biol. **244**, 680–691 (2007)
60. Sherratt, J.A., Lord, G.J.: Nonlinear dynamics and pattern bifurcations in a model for vegetation stripes in semi-arid environments. Theor. Popul. Biol. **71**, 1–11 (2007)
61. Epstein, I.R., Showalter, K.: Nonlinear chemical dynamics: oscillations, patterns and chaos. J. Phys. Chem. **100**, 13132–13147 (1996)
62. Vanag, V.K., Epstein, I.R.: Design and control of patterns in reaction–diffusion systems. Chaos **18**(2), 026107 (2008)
63. Kapral, R., Showalter, K. (ed.): Chemical Waves and Patterns. Springer, New York (1995)
64. Bordyugov, G., Fischer, N., Engel, H., Manz, N., Steinbock, O.: Anomalous dispersion in the Belousov-Zhabotinsky reaction: experiments and modeling. Physica D **239**, 766–775 (2010)
65. Krug, H.-J., Pohlmann, L., Kuhnert, L.: Analysis of the modified complete Oregonator accounting for oxygen sensitivity and photosensitivity of Belousov–Zhabotinsky reaction. J. Phys. Chem. **94**, 4862–4865 (1990)